

## H91 $\alpha$ RADIO RECOMBINATION LINE AND 3.5 CM CONTINUUM OBSERVATIONS OF THE PLANETARY NEBULA NGC 3242

Luis F. Rodríguez and Yolanda Gómez

Centro de Radioastronomía y Astrofísica, UNAM, Morelia

and

J. Alberto López, Ma. Teresa García-Díaz and David M. Clark

Instituto de Astronomía, UNAM, Ensenada

*Received October 31, 2018; accepted Year Month Day*

### RESUMEN

Presentamos observaciones de alta sensibilidad de la línea de recombinación de radio H91 $\alpha$  a 3.5 cm y de su continuo adyacente hacia la nebulosa planetaria NGC 3242. La temperatura electrónica derivada suponiendo equilibrio termodinámico local es consistente dentro de  $\sim 10\%$  con la determinada de líneas ópticas y de la discontinuidad de Balmer. La emisión de línea y la de continuo tienen una distribución espacial muy similar, indicando que a esta longitud de onda no hay otro proceso de emisión de continuo presente de manera significativa. En particular concluimos que la emisión de polvo rotante no es importante a esta longitud de onda. En esta línea de recombinación de radio la nebulosa presenta una estructura en velocidad radial consistente con la obtenida de observaciones de líneas en el visible.

### ABSTRACT

We present high sensitivity H91 $\alpha$  and 3.5 cm radio continuum observations toward the planetary nebula NGC 3242. The electron temperature determined assuming local thermodynamic equilibrium is consistent within  $\sim 10\%$  with that derived from optical lines and the Balmer discontinuity. The line emission and the continuum emission have very similar spatial distribution, suggesting that at this wavelength there is no other continuum process present in a significant manner. In particular, we conclude that emission from spinning dust is not important at this wavelength. In this radio recombination line the nebula presents a radial velocity structure consistent with that obtained from observations of optical lines.

*Key Words:* **PLANETARY NEBULAE: INDIVIDUAL (NGC 3242) — RADIATION MECHANISMS: THERMAL**

### 1. INTRODUCTION

NGC 3242 (PN G261.0+32.0) is a multiple-shell, attached-halo planetary nebula (PN), located at a distance of about 1 kpc (Stanghellini & Pasquali 1995). Recently, an expansion distance measured with radio continuum observations (Hajian, Phillips, & Terzian 1995) placed this PN at  $0.42 \pm 0.16$  kpc. As it is commonly the case in planetary nebula, the individual distances show a large spread, ranging from 0.28 to 2.0 kpc for NGC 3242 (Acker et al. 1992). We will adopt the distance of 1 kpc pro-

posed by Stanghellini & Pasquali (1995). The inner and outer shells of the object have diameters of 15" and 29", respectively. NGC 3242 is a high-excitation planetary nebula (class 7; Pottasch 1984) powered by a  $\geq 1000 L_{\odot}$  (Stanghellini & Pasquali 1995) SD0 star (Heap 1986) with a surface temperature of  $T_{eff} = 60,000$  K (Acker et al. 1992). The post-AGB mass of the central star is estimated to be  $M_{cs} = 0.56 \pm 0.01 M_{\odot}$ , corresponding to a main-sequence mass of  $M_{ms} = 1.2 \pm 0.2 M_{\odot}$  (Galli et al. 1997).

NGC 3242 was the first PN with a firm detection of the  $^3\text{He}^+$  hyperfine line at 8.665 GHz (Balsler, Rood, & Bania 1999). As part of these  $^3\text{He}^+$  studies, the Very Large Array archive contains also high quality, unpublished data of the H91 $\alpha$  radio recombination line (project AR271), that has a nearby rest frequency of 8.584 GHz. In this paper we analyze this radio recombination line and the adjacent continuum. The motivation of this analysis is in first place to study the radio recombination line emission of this planetary nebula at interferometer angular resolutions since to our knowledge only single dish observations have been published. The second reason to study the continuum and radio recombination line emission of this PN is that recently (Casassus 2005; 2007) it was proposed as one of the planetary nebulae that may show excess anomalous microwave emission (e. g. Casassus et al. 2004; Finkbeiner et al. 2002). This new continuum radiation mechanism has been attributed to electric dipole emission from rapidly rotating dust grains ("spinning dust"), as predicted by Draine & Lazarian (1998). In a nebula that is optically thin at centimeter wavelengths one expects the free-free continuum emission and the radio recombination line emission to be very similar since both originate mostly from electron-proton interactions. The significant presence of an independent radiation mechanism such as spinning dust emission is expected to become evident in a careful comparison between the total continuum and the radio recombination line emissions.

## 2. OBSERVATIONS

The observations were made at 3.5 cm during 1992 August 15 in the D configuration of the VLA of the NRAO<sup>1</sup>. The frequency of the observations was centered at the rest frequency of the H91 $\alpha$  radio recombination line, 8.584 GHz. The source 1331+305 was used as an absolute amplitude calibrator (with an adopted flux density of 5.10 Jy). The source 1035-201 was used as the phase calibrator (with a bootstrapped flux density of  $0.563 \pm 0.007$  Jy) and the source 0542+498 was used as the bandpass calibrator (with a bootstrapped flux density of  $4.370 \pm 0.039$  Jy). The observations were made with 31 spectral line channels with a frequency resolution of 195.3 kHz (corresponding to  $6.8 \text{ km s}^{-1}$ ). A continuum channel (the channel 0) contains the average of the central 75% of the available band. The data were calibrated following the standard VLA procedures

<sup>1</sup>The National Radio Astronomy Observatory is operated by Associated Universities Inc. under cooperative agreement with the National Science Foundation.

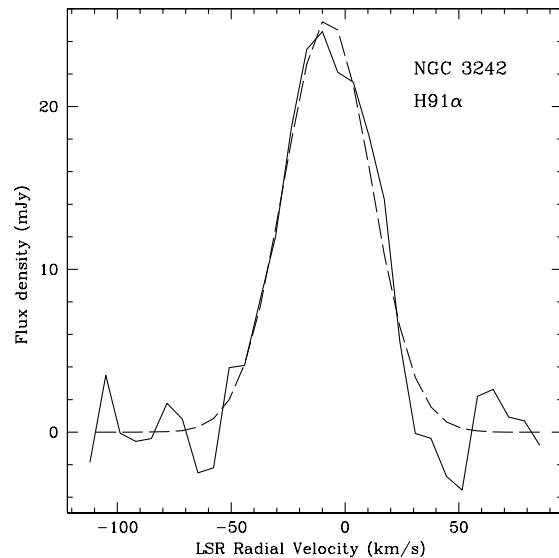


Fig. 1. Integrated H91 $\alpha$  line emission from the planetary nebula NGC 3242. The dashed line is the least-squares fitted Gaussian profile. The parameters of the fit are given in Table 1.

for spectral line, using the software package AIPS of NRAO. Using the channel 0, the data were self-calibrated in amplitude and phase. The images were made with natural weighting to obtain the highest sensitivity. The synthesized beam has half power full width dimensions of  $13''0 \times 8''4$ , with the major axis at a position angle of  $+10^\circ$ .

## 3. INTERPRETATION AND RESULTS

### 3.1. Average LTE Electron Temperature

In Figure 1 we show the total H91 $\alpha$  line emission, integrated on a box of solid angle  $53'' \times 61''$  ( $\Delta\alpha \times \Delta\delta$ ) that includes all the bright emission from the ionized nebula. The integrated parameters for line and continuum in this box are given in Table 1. The continuum parameters were derived from an image made using 14 channels in the spectrum that were considered to be free of line emission.

The electron temperature for an optically thin plasma, assuming LTE, is given by:

$$T_e^* = \left[ 7.23 \times 10^3 \nu^{1.1} \frac{S_C}{\Delta\nu S_L (1+y^+)} \right]^{0.87},$$

where  $T_e^*$  is the LTE electron temperature in K,  $\nu$  is the observing frequency in GHz,  $S_C$  is the continuum flux density in mJy,  $\Delta\nu$  is the half maximum full width of the line in  $\text{km s}^{-1}$ ,  $S_L$  is the peak line flux

TABLE 1

CONTINUUM AND H91 $\alpha$  LINE PARAMETERS  
FOR NGC 3242

Parameter <sup>a</sup>	Value
$S_C$	$660 \pm 10$ mJy
$S_L$	$25.4 \pm 1.1$ mJy
$\Delta v$	$45.2 \pm 2.3$ km s <sup>-1</sup>
$v_{LSR}$	$-7.6 \pm 1.0$ km s <sup>-1</sup>

<sup>a</sup> $S_C$  = Continuum Flux Density,  $S_L$  = Peak Line Flux Density,  $\Delta v$  = Half Maximum Full Width,  $v_{LSR}$  = LSR Radial Velocity.

density in mJy, and  $y^+ = He^+/H^+$  is the ionized helium to ionized hydrogen ratio, that we take equal to 0.1 (Balser et al. 1999). Using the values given in Table 1 and in the text, we obtain an electron temperature of  $T_e^* = 10,100 \pm 700$  K. This value is in good agreement with the average values determined from optical lines. Kaler (1986) lists nine independent determinations of the electron temperature that range from 10,060 to 12,300 K, with an average value of  $11,200 \pm 600$  K, that overlaps within error our radio determination. More recent electron temperature determinations from the Balmer discontinuity and optical forbidden lines are also consistent with this range (Liu & Danziger 1993; Krabbe & Copetti 2005; Pottasch & Bernard-Salas 2008).

We note that the assumption that NGC 3242 is optically thin at 8.6 GHz is well justified because the flux density determined by us (660 mJy) is similar to those determined by Condon & Kaplan (1998) at 1.4 GHz (760 mJy), by Griffith et al. (1994) at 4.9 GHz (745 mJy), by Kaftan-Kassim (1966) at 5.0 GHz (760 mJy) and by Heckathorn (1971) at 10.6 GHz (600 mJy), indicating that we are in the “flat”, optically-thin part of the free-free spectrum.

### 3.2. Comparison between the spatial distribution of the continuum emission and the line emission

The good agreement of the radio-determined electron temperature with the values from optical measurements would seem to suggest that NGC 3242 does not have a significant continuum excess from spinning dust, since in this case our estimate using the electron temperature formula given above would have resulted in an electron temperature much larger than that obtained in the optical measurements.

There are, however, two important considerations that we discuss in what follows. An important caveat is that the continuum excess from spinning

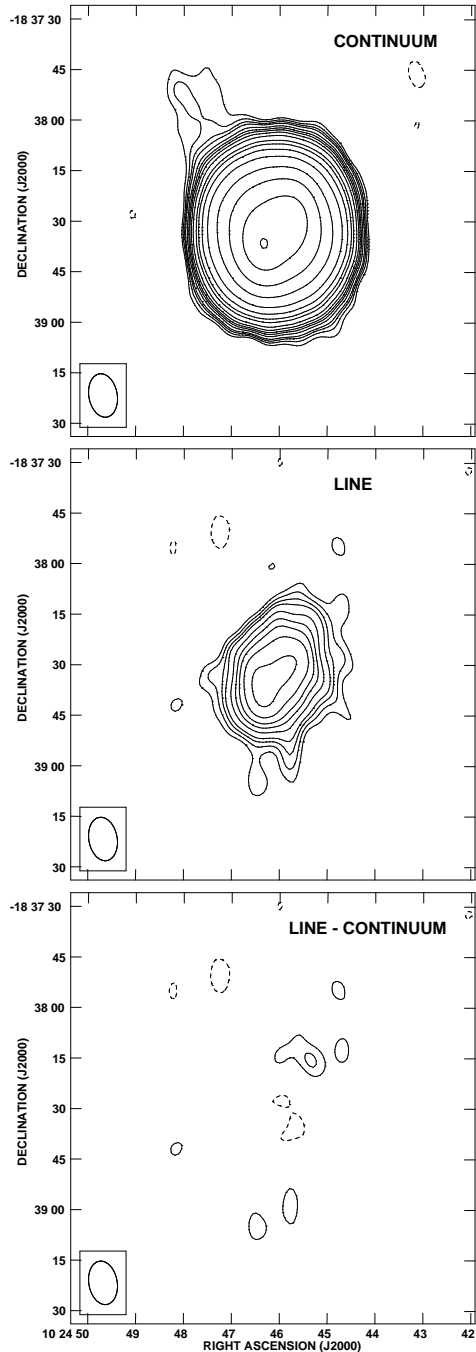


Fig. 2. Contour images of the 3.5 cm continuum emission (top), the integrated H91 $\alpha$  line emission (middle), and the integrated line emission minus continuum difference image (bottom), made as explained in the text. The contours are -3, 3, 4, 5, 6, 8, 10, 12, 15, 20, 30, 40, 60, 100, 200, 400, 800, and 1200 times the rms noise of the images that is  $0.11$  mJy beam<sup>-1</sup> for the top image and  $8.5$  mJy beam<sup>-1</sup> km s<sup>-1</sup> for the middle and bottom images.

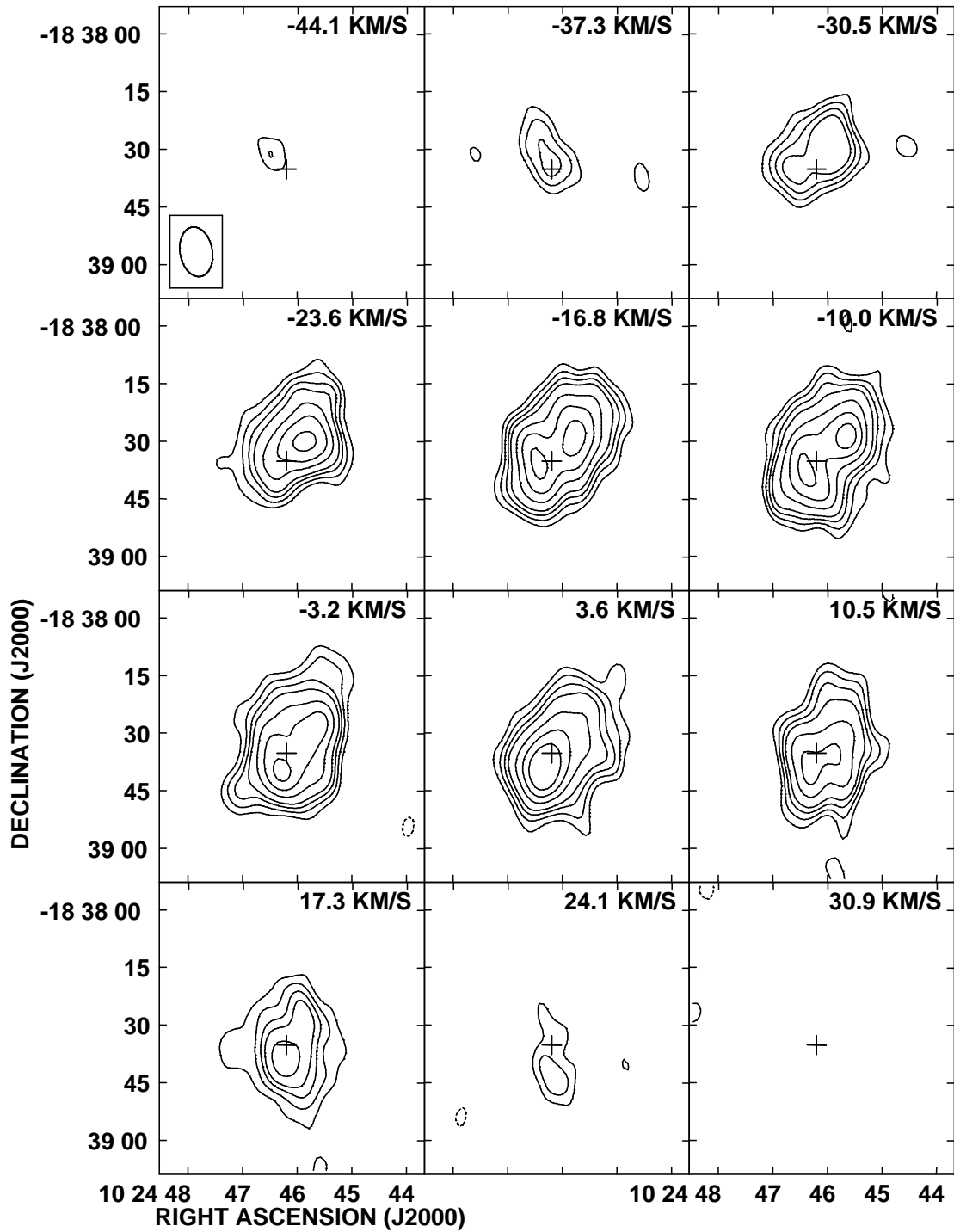


Fig. 3. Channel line images of the H91 $\alpha$  emission from NGC 3242. The contours are -5, -4, -3, 3, 4, 5, 6, 8, 10, 12, 15, 20, and 30 times  $2.04 \mu\text{Jy km s}^{-1}$ , the rms noise of the individual images. The LSR radial velocity of each image is labeled in the top right corner. The cross marks the peak position of the continuum emission. The half power contour of the restoring beam ( $13''.0 \times 8''.4$ ;  $PA = +10^\circ$ ), is shown in the bottom left corner of the panel at  $-44.1 \text{ km s}^{-1}$ .

dust is believed to be stronger in the 10 to 30 GHz band and that it may not be present at detectable levels at 8.6 GHz.

A second consideration that can also be argued is that, even if the spinning dust emission is present, non-LTE effects may enhance the radio recombination line (Dupree & Goldberg 1970) in such a way that this enhancement approximately compensates for the continuum increase resulting in that the derived LTE electron temperature gives a value similar to that expected from the optical observations. Fortunately, we can further test this latter possibility. In a nebula that is optically thin at centimeter wavelengths, like NGC 3242, one expects the free-free continuum emission and the radio recombination line emission to distribute in the sky in a very similar manner, since both originate basically from electron-proton interactions. An independent radiation mechanism such as spinning dust emission is not expected to have an intensity distribution on the sky that follows that of the ionized gas and, if present, this extra component is expected to become evident in a careful comparison between the total continuum and the radio recombination line emissions.

In Figure 2 we present images of the continuum and integrated line emission from NGC 3242. The integrated line emission image was made adding the channels from  $-44.1$  to  $+24.1$   $\text{km s}^{-1}$ . From a simple comparison of the images it is not possible to say how different are the two images because of the much larger signal-to-noise ratio of the continuum image, that allows to contour much more extended structure. A first indication that the continuum and the line emissions are very similar comes from determining their deconvolved angular dimensions using the task JMFIT of AIPS. For the continuum emission we obtain  $16''.0 \pm 0''.1 \times 12''.0 \pm 0''.1$ ;  $PA = 116^\circ \pm 1^\circ$ , while for the line emission we obtain  $16''.1 \pm 0''.6 \times 11''.8 \pm 0''.1$ ;  $PA = 118^\circ \pm 7^\circ$ . The deconvolved dimensions overlap within the error.

To test more quantitatively how different the two emissions are, we present in a third panel the difference of the integrated line and continuum images, with the continuum image scaled (by a factor of 0.036) to have the same flux density as the integrated line image. As can be seen in the difference image, there is no clear signature of a residual emission that could trace a mechanism with a different spatial distribution to that of the free-free continuum or integrated line emissions. The residuals of the difference image are at a  $\sim 15\%$  level of the integrated line image and we rule out the presence of a significant contribution from a different mechanism

at this level and at sizes comparable or smaller than the largest angular scales detectable by the VLA at 3.6 cm in the D configuration ( $\sim 3'$ ).

Our results are consistent with those of Pazderska et al. (2009; see also Umana et al. 2008), who failed to find excess continuum emission at 30 GHz in their survey of planetary nebulae and concluded that free-free emission alone can explain the observed spectra.

### 3.3. Nebular kinematics

#### 3.3.1. Radio Observations

We can also use the H91 $\alpha$  observations to discuss the kinematics of the nebula, although at the moderate angular resolution of these observations ( $\sim 10''$ ). In Figure 3 we show the individual channel line emission over the velocity range where there is detectable signal. At negative LSR radial velocities, the strongest emission comes from the NW part of the nebula, and as we progress to positive LSR radial velocities the line emission shifts to the SE (see Fig. 3).

#### 3.3.2. Optical Observations

High resolution spectroscopic observations of NGC 3242 were obtained at the Observatorio Astronómico Nacional at San Pedro Mártir, México on 2009, January 15 as part of the San Pedro Mártir kinematic catalog of planetary nebulae (López et al. 2006). The data were obtained with the Manchester Echelle Spectrometer (MES-SPM) (Meaburn et al. 2003) on the 2.1 m telescope in a  $f/7.5$  configuration. This instrument is equipped with a SITE CCD detector with  $1024 \times 1024$  square pixels, each  $24 \mu\text{m}$  on a side. We used a  $90 \text{ \AA}$  bandwidth filter to isolate the 87th order containing the H $\alpha$  and [N II] nebular emission lines. Two times binning was employed in both the spatial and spectral directions. Consequently, 512 increments, each  $0''.624$  long gave a projected slit length of  $5'.32$  on the sky. We used a slit of  $150 \mu\text{m}$  wide ( $\equiv 11 \text{ km s}^{-1}$  and  $1''.9$ ) oriented along the major axis of the nebula at a P.A. of  $-30^\circ$ , and located just west of the central star. The exposure time was 1800 s and the spectrum was calibrated in wavelength against the spectrum of a Th/Ar arc lamp to an accuracy of  $\pm 1 \text{ km s}^{-1}$  when converted to radial velocity. The bi-dimensional emission line spectra or position – velocity (p- v) arrays for both H $\alpha$  and [N II]  $\lambda 6584 \text{ \AA}$  are shown in Figure 4. Here the north-west corresponds to top of the profile and the south-east to the bottom of the figure.

As it is well known, NGC 3242 is a multi-shell elliptical nebula (Meaburn et al. 2000) with fast, low ionization emission knots or FLIERs (Balick et al.

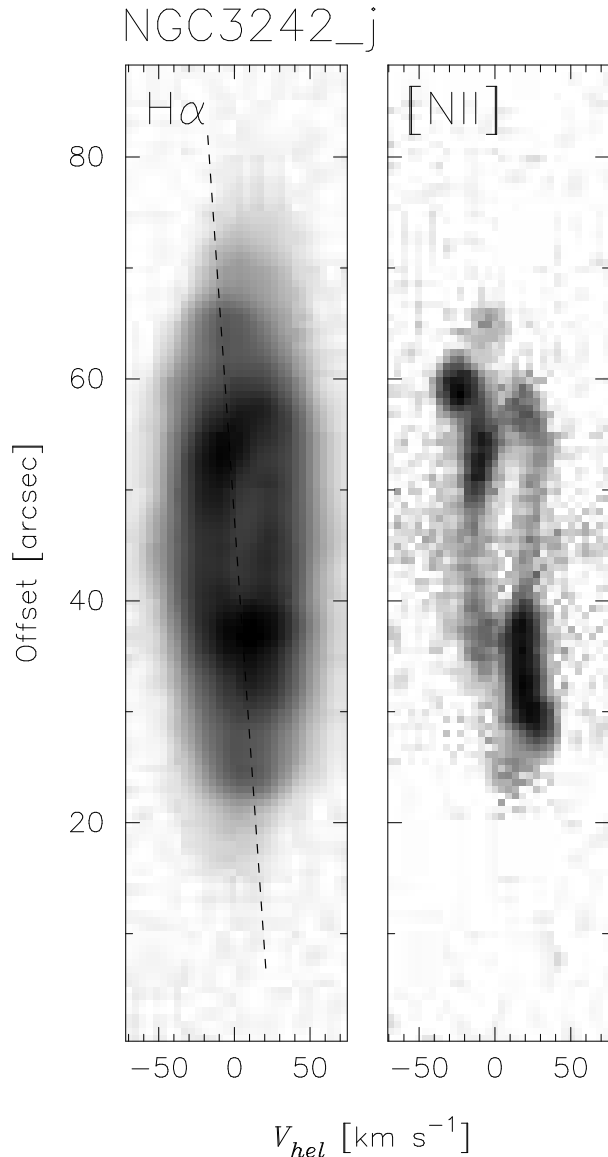


Fig. 4.  $H\alpha$  and  $[N\ II] \lambda 6584 \text{ \AA}$  bi-dimensional emission line spectra. The long-slit is oriented at a P.A. of  $-30^\circ$  with north-west to top of the figure and south-east at the bottom. The dashed line in the  $H\alpha$  line profile highlights the velocity tilt present in the bipolar outflow. The bright knots in the  $[N\ II] \lambda 6584 \text{ \AA}$  correspond to the FLIERS. In the direction of NGC 3242 the heliocentric and LSR radial velocities are related by  $v_{hel} = v_{LSR} + 10.2 \text{ km s}^{-1}$ .

1993) located at the leading edges of a mild bipolar outflow that emerges from the nucleus. The emission line profiles shown in Figure 4 clearly reveal the main inner components of this nebula that are apparent in public *Hubble Space Telescope* images. Namely, in the  $H\alpha$  p-v array the main bright bubble is observed as the main velocity ellipse and the tilted bipolar outflow that is indicated in the figure by a dashed line, both elements coincide with the kinematics mapped by our radio recombination line observations. A tenuous, more extended halo is also present as part of the p-v array. The  $[N\ II] \lambda 6584 \text{ \AA}$  p-v array shows the main bright bubble and the external knots corresponding to the FLIERS. Clearly the tilted bipolar outflow found in the  $H\alpha$  and the  $H91\alpha$  line emissions follows the bipolar outflow that trails and surrounds the FLIERS.

#### 4. CONCLUSIONS

We presented VLA observations of the  $H91\alpha$  radio recombination line and the adjacent continuum, as well as of  $H\alpha$  and  $[N\ II] \lambda 6584 \text{ \AA}$ , toward the planetary nebula NGC 3242. Our main conclusions can be summarized as follows.

1. The LTE electron temperature derived from the line to continuum ratio agrees well with the values derived in the optical.
2. The spatial distribution of continuum and line emission are very similar, arguing against the presence of significant continuum contamination from spinning dust emission.
3. The radial velocity structure found from the  $H91\alpha$  line is consistent with that derived from the optical lines.

We thank S. Casassus for valuable comments. We acknowledge the support of DGAPA, UNAM, and of CONACyT (México). This research has made use of the SIMBAD database, operated at CDS, Strasbourg, France.

#### REFERENCES

- Acker, A., Marcout, J., Ochsenbein, F., Stenholm, B., & Tylenda, R. 1992, *Strasbourg-ESO Catalogue of Galactic Planetary Nebulae*, ESO, Garching
- Balser, D. S., Rood, R. T., & Bania, T. M. 1999, *ApJ*, 522, L73
- Balick, B., Rugers, M., Terzian, Y. & Chungalur, J. N. 1993, *ApJ*, 411, 778
- Casassus, S., Readhead, A. C. S., Pearson, T. J., Nyman, L.-Å., Shepherd, M. C., & Bronfman, L. 2004, *ApJ*, 603, 599
- Casassus, S. 2005, in *ASP Conference Series 344, The Cool Universe: Observing Cosmic Dawn*, ed. C. Lidman & D. Alloin (San Francisco: ASP), 140

- Casassus, S., Nyman, L.-Å., Dickinson, C., & Pearson, T. J. 2007, *MNRAS*, 382, 1607
- Condon, J. J., & Kaplan, D. L. 1998, *ApJS*, 117, 361
- Draine, B. T., & Lazarian, A. 1998, *ApJ*, 508, 157
- Dupree, A. K., & Goldberg, L. 1970, *ARA&A*, 8, 231
- Finkbeiner, D. P., Schlegel, D. J., Frank, C., & Heiles, C. 2002, *ApJ*, 566, 898
- Galli, D., Stanghellini, L., Tosi, M., & Palla, F. 1997, *ApJ*, 477, 218
- Griffith, M. R., Wright, A. E., Burke, B. F., & Ekers, R. D. 1994, *ApJS*, 90, 179
- Hajian, A. R., Terzian, Y., & Bignell, C. 1995, *AJ*, 109, 2600
- Heap, S. R. 1986, in *Proc. Intl. Symp., New Insights in Astrophysics, Eight Years of UV Astronomy with IUE*, ed. E. Rolfe (ESA SP-263; Noordwijk: ESA), 291
- Heckathorn, J. 1971, *Ap&SS*, 11, 309
- Kaftan-Kassim, M. A. 1966, *ApJ*, 145, 658
- Kaler, J. B. 1986, *ApJ*, 308, 322
- Krabbe, A. C., & Copetti, M. V. F. 2005, *A&A*, 443, 981
- Liu, X.-W., & Danziger, J. 1993, *MNRAS*, 263, 256
- López, J. A., Richer, M. G., Riesgo, H., Steffen, W., García-Segura, G., Meaburn, J. & Bryce, M. 2006, in *Planetary Nebulae in our Galaxy and Beyond*, IAU Symp. 234, Cambridge University Press, eds. Barlow, M. J. & Méndez, R. H., pp 21-24
- Meaburn, J., López, J. A., & Noriega-Crespo, A. 2000, *ApJS*, 128, 321
- Meaburn, J., López, J. A., Gutiérrez, L., Quiróz, F., Murillo, J. M. & Valdéz, J. 2003, *RMxAA*, 39, 185
- Pazderska, B. M., et al. 2009, *A&A*, 498, 463
- Pottasch, S. R. 1984, *Planetary Nebulae* (Dordrecht: Reidel)
- Pottasch, S. R., & Bernard-Salas, J. 2008, *A&A*, 490, 715
- Stanghellini, L., & Pasquali, A. 1995, *ApJ*, 452, 286
- Umana, G., Leto, P., Trigilio, C., Buemi, C. S., Manzitto, P., Toscano, S., Dolei, S., & Cerrigone, L. 2008, *A&A*, 482, 529

Yolanda Gómez and Luis F. Rodríguez: Centro de Radioastronomía y Astrofísica, UNAM, A. P. 3-72, (Xangari), 58089 Morelia, Michoacán, México (y.gomez; l.rodriguez@crya.unam.mx).

David M. Clark, Ma. Teresa García-Díaz, and J. Alberto López: Instituto de Astronomía, Universidad Nacional Autónoma de México Campus Ensenada, Ensenada, Baja California, 22800, México (jal; tere; dm-clark@astroesen.unam.mx).